JACS
JOURNAL OF THE AMERICAN CHEMICAL SOCIETY
Article
pubs.acs.org/JACS

# Isolation and Crystallographic Characterization of $La_2C_2@C_s(574)$-$C_{102}$ and $La_2C_2@C_2(816)$-$C_{104}$: Evidence for the Top-Down Formation Mechanism of Fullerenes

Wenting Cai, Fang-Fang Li, Lipiao Bao, Yunpeng Xie, and Xing Lu*

State Key Laboratory of Materials Processing and Die & Mold Technology, School of Materials Science and Engineering, Huazhong University of Science and Technology (HUST), Wuhan 430074, China

Supporting Information

**ABSTRACT:** Tubular higher fullerenes are prototypes of finite-length end-capped carbon nanotubes (CNTs) whose structures can be accurately characterized by single-crystal X-ray diffraction crystallography. We present here the isolation and crystallographic characterization of two unprecedented higher fullerenes stabilized by the encapsulation of a $La_2C_2$ cluster, namely, $La_2C_2@C_s(574)$-$C_{102}$, which has a perfect tubular cage corresponding to a short (10, 0) zigzag carbon nanotube, and $La_2C_2@C_2(816)$-$C_{104}$ which has a defective cage with a pyracylene motif inserting into the cage waist. Both cages provide sufficient spaces for the large $La_2C_2$ cluster to adopt a stretched and nearly planar configuration, departing from the common butterfly-like configuration which has been frequently observed in midsized carbide metallofullerenes (e.g., $Sc_2C_2@C_{80-84}$), to achieve strong metal−cage interactions. More meaningfully, our crystallographic results demonstrate that the defective cage of $C_2(816)$-$C_{104}$ is a starting point to form the other three tubular cages known so far, i.e., $D_5(450)$-$C_{100}$, $C_s(574)$-$C_{102}$, and $D_{3d}(822)$-$C_{104}$, presenting evidence for the top-down formation mechanism of fullerenes. The fact that only the large $La_2C_2$ cluster has been found in giant fullerene cages ($C_{>100}$) and the small clusters $M_2C_2$ (M = Sc, Y, Er, etc.) are present in midsized fullerenes ($C_{80}$−$C_{86}$) indicates that geometrical matching between the cluster and the cage, which ensures strong metal−cage interactions, is an important factor controlling the stability of the resultant metallofullerenes, in addition to charge transfer.

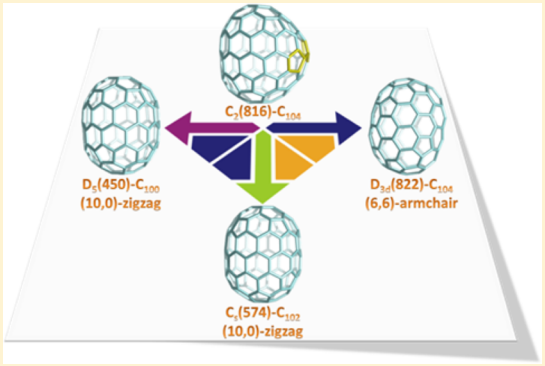


## 1. INTRODUCTION

Fullerenes are defined as spherical molecules consisting of hexagonal and pentagonal carbon rings. However, experimental results of a series of higher fullerenes such as $C_{80}$ and $C_{90}$ showed that their cages present tubular appearances that are in clear connections with finite-length capped carbon nanotubes.[1−3] So far, the studies of tubular fullerenes have focused on those with a cage size ranging from $C_{70}$ to $C_{96}$.[2−5] For fullerenes with even larger cages such as $C_{2n}$ ($2n \geq 100$), the existence of numerous isomers and their poor solubility in common solvents hinder the isolation of pure samples and the characterization of their molecular structures. One effective strategy used to capture giant tubular fullerenes is exohedral modification. For instance, some giant fullerenes can be obtained as their chlorinated derivatives such as $C_{100}(18)$-$Cl_{28/30}$, $C_{102}(603)Cl_{18/20}$, $C_{104}(234)Cl_{22}$, and $C_{104}(812)$-$Cl_{24}$.[6−10] However, the functionalized cages are severely distorted by the abundant addition groups, and some structures undergo skeletal transformation and thus derive from the original cages.

Another obstacle in the research of higher fullerenes $C_{2n}$ ($2n \geq 100$) is the low stability of giant tubular cages. For example, computational results suggested that none of the 10 most stable isolated-pentagon-rule (IPR) isomers of neutral $C_{106}$ tend to possess a tubular cage with the bands of contiguous hexagons.[11] However, it was predicted that some giant tubular fullerenes are stable as their tetra-anions or hexa-anions.[12,13] In this regard, endohedral metal doping presents as another practical way for the stabilization of giant tubular fullerenes because of the transfer of a certain amount of electrons from the encapsulated metallic species to the fullerene cage.[14] More meaningfully, endohedral metal doping does not change the cage framework, and thus, the resultant molecules largely keep the inherent properties of pristine fullerenes. Indeed, some giant tubular cages have been obtained in the form of endohedral metallofullerenes (EMFs).[15] For example, two giant nanotubular fullerenes $C_{100}$ and $C_{104}$ were obtained by encapsulating either a $La_2$ cluster or a $Sm_2$ cluster, respectively, forming $La_2@D_5(450)$-$C_{100}$ and $Sm_2@D_{3d}(822)$-$C_{104}$ which have been structurally characterized with X-ray crystallography.[16,17] It is believed that the internal cluster transfers either 4 (for $Sm_2@D_{3d}(822)$-$C_{104}$) or 6 (for $La_2@D_5(450)$-$C_{100}$) electrons to the respective cage to stabilize it. Recently, we found that the

Received: April 16, 2016
Published: May 9, 2016





DOI: 10.1021/jacs.6b03934
J. Am. Chem. Soc. 2016, 138, 6670−6675

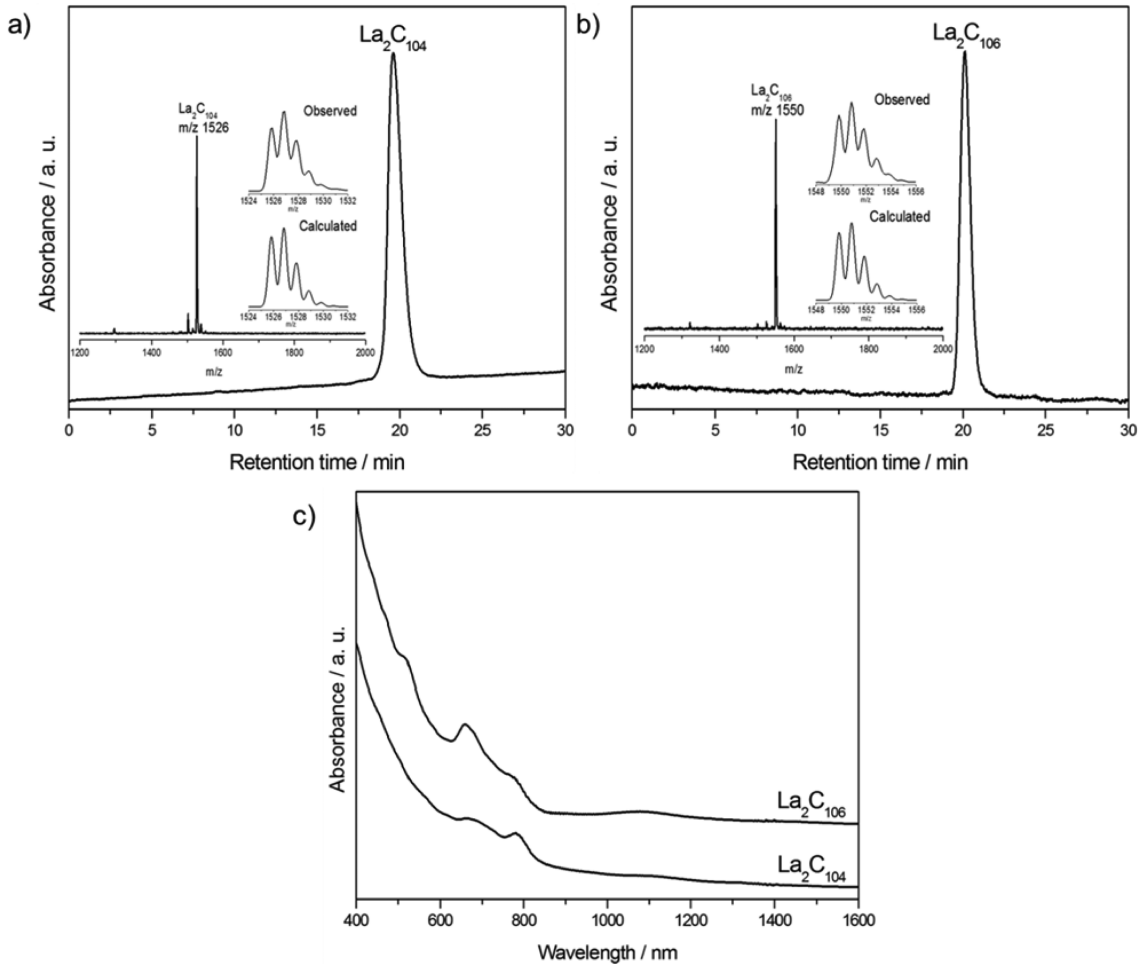


**Figure 1.** HPLC chromatograms of purified (a) $La_2C_{104}$ and (b) $La_2C_{106}$ on a Buckyprep column with chlorobenzene as the eluent. (HPLC conditions: flow rate, 0.7 mL $min^{-1}$; detection wavelength, 330 nm. Insets show the LDI-TOF mass spectra and expansions of the observed isotopic distributions of $La_2C_{104}$ and $La_2C_{106}$ in comparison with the calculated ones, respectively.) (c) Vis−NIR absorption spectra of purified $La_2C_{104}$ and $La_2C_{106}$ in chlorobenzene.

tubular $D_5(450)$-$C_{100}$ cage is also suitable for encapsulating a $La_2C_2$ cluster featuring a 4-electron-transfer process.[18] Interestingly, it was discovered that the encapsulated $La_2C_2$ cluster exhibits a strong metal−cage interaction that induces an anomalous axial compression of the $D_5(450)$-$C_{100}$ cage, instead of expanding it. Moreover, the $La_2C_2$ cluster adopts a twisted configuration inside $D_5(450)$-$C_{100}$, in contrast to the commonly encountered butterfly-like configuration of $M_2C_2$ (M = Sc, Y, Er, etc.)[19] in midsized fullerenes (e.g., $C_{80}$−$C_{84}$). Since theoretical calculations have predicted that the $M_2C_2$ cluster tends to adopt a linear configuration, when the cage size increases,[20,21] we speculate that the large $La_2C_2$ cluster would facilitate templating giant tubular cages even larger than $C_{100}$, and the extremely long axis of these tubular cages would provide sufficient space for the cluster to adopt a linear configuration.

Herein we report the isolation and single-crystal X-ray crystallographic characterizations of two unprecedented giant fullerenes containing a lanthanum carbide cluster, namely, $La_2C_2$@$C_s(574)$-$C_{102}$ and $La_2C_2$@$C_2(816)$-$C_{104}$. The former possesses an ideal tubular cage corresponding to a short (10, 0) zigzag CNT, and the latter has a pyracylene "defect" inserting into the cage waist. The $La_2C_2$ cluster is more favorable to adopt a stretched and nearly planar configuration in these two cages. In addition, we discover with X-ray crystallography that the defective cage, $C_2(816)$-$C_{104}$, can be a starting point to form the other three ideal tubular cages known so far, i.e., $D_5(450)$-$C_{100}$, $C_s(574)$-$C_{102}$, and $D_{3d}(822)$-$C_{104}$, by elimination of the pyracylene motif following different pathways, presenting evidence for the top-down formation mechanism of fullerenes during the arc discharge process.

## 2. RESULTS AND DISCUSSION

**Isolation and Characterizations of $La_2C_2$@$C_s(574)$-$C_{102}$ and $La_2C_2$@$C_2(816)$-$C_{104}$.** Soot containing La-EMFs was synthesized with a direct-current arc discharge method, and these materials were extracted with 1,3,5-trichlorobenzene (TCB). Multistage HPLC separations gave pure isomers of $La_2C_{104}$ and $La_2C_{106}$ (Figures S1−S5, Supporting Information). Figure 1 shows the chromatograms and mass spectra of the purified samples. The vis−NIR spectra of these two compounds are shown in Figure 1c. Their spectral onsets both locate at around 1300 nm, resulting in small HOMO−LUMO gaps. $La_2C_{104}$ displays absorption bands at 774 and 664 nm, and $La_2C_{106}$ exhibits distinct absorptions at 1099, 766, 655, and 515 nm.

The molecular structures of $La_2C_{104}$ and $La_2C_{106}$ are unambiguously determined with single-crystal X-ray diffraction.


DOI: 10.1021/jacs.6b03934
J. Am. Chem. Soc. 2016, 138, 6670−6675

Similar to the case of $La_2C_2@D_5(450)$-$C_{100}$,[18] neither of these endohedrals are cocrystallized with $Ni^{II}$(OEP) (OEP = 2, 3, 7, 8, 12, 13, 17, 18-octaethylporphin dianion) molecules although a benzene solution of $Ni^{II}$(OEP) and a $CS_2$ solution of the fullerene have been used for the single-crystal growth. The crystal units contain only one metallofullerene molecule and two or three $CS_2$ molecules (Figure S6, Supporting Information), analogous to the fullerene solvates obtained by evaporation of solutions,[6,22,23] suggesting that the tubular appearance of the cages can facilitate the formation of neat crystals without the assistance of cocrystallization reagents.

Figure 2a,b show that both compounds are actually carbide cluster EMFs, i.e., $La_2C_2@C_s(574)$-$C_{102}$ and $La_2C_2@C_2(816)$-$C_{104}$ (nomenclature in accordance with the spiro algorithm[24]). A notable feature of the carbon cage of $La_2C_2@C_s(574)$-$C_{102}$ is the existence of two bands of 10 contiguous hexagons that encircle the cage, similar to the previously reported tubular $D_{3d}(822)$-$C_{104}$,[16] $D_5(450)$-$C_{100}$,[17] and $D_{5h}(1)$-$C_{90}$.[2] In contrast, $La_2C_2@C_2(816)$-$C_{104}$ has a pyracylene unit (highlighted in green in Figure 2b) inserting into the two bands of hexagons on the cage waist, reducing the cage symmetry to form a "defective" tubular structure.

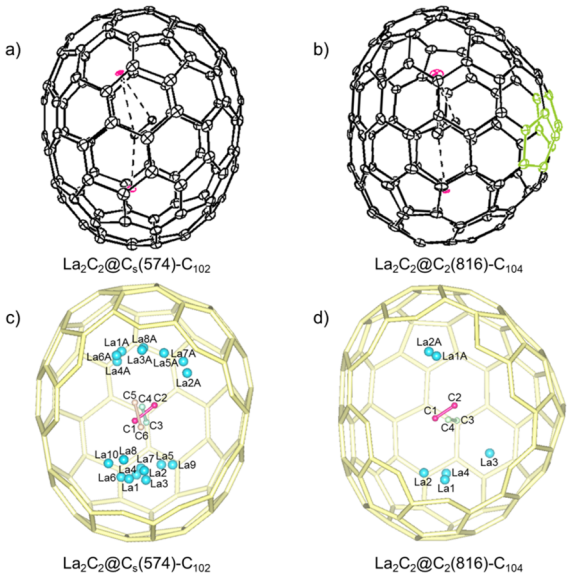


**Figure 2.** ORTEP drawings of (a) $La_2C_2@C_s(574)$-$C_{102}$ and (b) $La_2C_2@C_2(816)$-$C_{104}$. Thermal ellipsoids are shown at the 10% probability level. Only the major fullerene cage and the predominant carbide cluster are shown, whereas minor sites and solvent molecules are omitted for clarity. The pyracylene motif in $La_2C_2@C_2(816)$-$C_{104}$ is highlighted in green. Perspective drawings show (c) 18 positions of the disordered lanthanum sites with respect to the $C_2$-unit in $La_2C_2@C_s(574)$-$C_{102}$ and (d) six positions of the disordered lanthanum sites with respect to the $C_2$-unit in $La_2C_2@C_2(816)$-$C_{104}$.

Inside the cage, the carbide clusters in both compounds show some degree of disorder (Figure 2c,d and Tables S1 and S2 in Supporting Information). In $C_s(574)$-$C_{102}$, 18 La positions are found for the two La atoms which are arranged in the form of an umbrella shape with respect to the three disordered positions of the $C_2$-unit (Figure 2c), whereas only six La positions are found for the two La atoms together with two disordered positions of the $C_2$-unit in $C_2(816)$-$C_{104}$ (Figure 2d). It seems that the free movement of the metal atoms is largely hindered in the defective $C_2(816)$-$C_{104}$ cage, as compared to the situations of $La_2C_2@D_5(450)$-$C_{100}$[17] and $La_2C_2@C_s(574)$-$C_{102}$ which have ideal tubular cages. It is well-known that pentagons are the sites of negative charges in fulleride anions and EMFs.[12,25] Therefore, the distribution of pentagons on a fullerene cage is a key factor that governs the location and even the motion of the metal ions. In this regard, the largely confined metal sites in $La_2C_2@C_2(816)$-$C_{104}$ should be a result of the existence of the pyracylene unit in the [10]cyclacene framework.

In spite of the disordered La positions and the $C_2$-unit, the predominant La ions in both $La_2C_2@C_s(574)$-$C_{102}$ and $La_2C_2@C_2(816)$-$C_{104}$ are separated, and the line between them is slightly displaced from the long axis of the respective fullerene cage (Figure 3a). One predominant La position in $La_2C_2@C_s(574)$-$C_{102}$ is arranged in the center of a hexagon, whereas the other one is situated over a [5, 6]-bond on the opposite. The major positions of the two La atoms in $La_2C_2@C_2(816)$-$C_{104}$ deviate from the pyracylene region with one locating around a [6, 6]-bond, and the other sitting over a [5, 6]-bond on the opposite side.

In both compounds, the $La_2C_2$ unit adopts a stretched and nearly planar configuration, similar to the structure of the relatively small $Sc_2C_2$ cluster in the large $C_{2v}(9)$-$C_{86}$,[26] but completely different from the situations in $Sc_2C_2@C_{2v}(5)$-$C_{80}$,

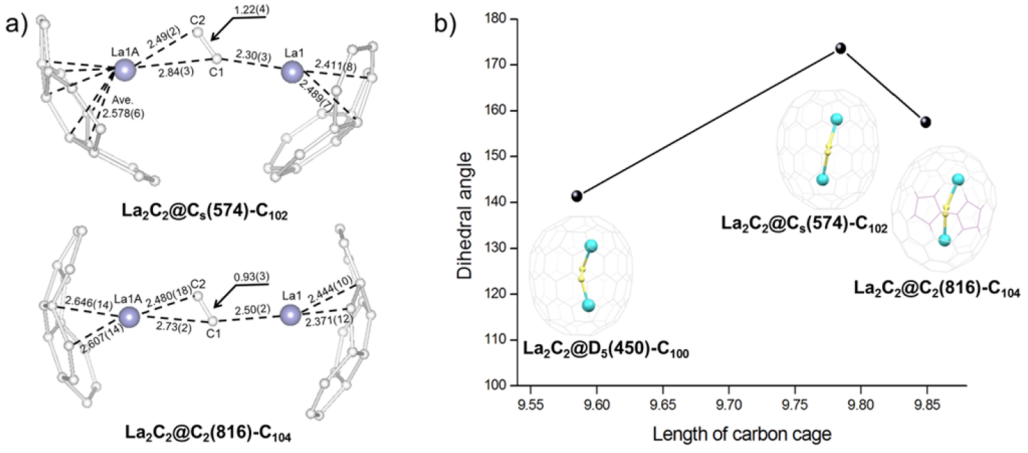


**Figure 3.** (a) Relative positions of the major $La_2C_2$ cluster to a partial cage of $La_2C_2@C_s(574)$-$C_{102}$ or $La_2C_2@C_2(816)$-$C_{104}$. (b) Geometric features of the encaged cluster and their dihedral angles between the two $La_2C_2$ planes against the cage length of $La_2C_2@C_{100,102,104}$.



DOI: 10.1021/jacs.6b03934
J. Am. Chem. Soc. 2016, 138, 6670−6675

$Sc_2C_2$@$C_{3v}$(8)-$C_{82}$, and $Sc_2C_2$@$D_{2d}$(23)-$C_{82}$ where the $Sc_2C_2$ cluster shows a bent butterfly-like configuration.[27] The disordered $C_2$ unit is no longer perpendicular to the line between the two predominant La positions. The La−C−C−La dihedral angles in $La_2C_2$@$C_s$(574)-$C_{102}$ and $La_2C_2$@$C_2$(816)-$C_{104}$ are 173.6° and 157.5°, respectively, which are much larger than that in $La_2C_2$@$D_5$(450)-$C_{100}$ (141.3°) (Figure 3b). A trend that the carbide cluster changes from a slightly bent structure to a nearly planar geometry with increasing of the cage length is observed. The anomalously small value of the La−C−C−La dihedral angle in $La_2C_2$@$C_2$(816)-$C_{104}$ should also be a result of the pyracylene "defect" which destroys the ideal tubular structure. In line with the theoretical predictions that the $M_2C_2$ cluster would adopt a linear configuration in large cages,[28] it is speculated that the nearly planar geometry of $La_2C_2$ found here should be an intermediate structure.

**Structural Rearrangements from $C_2$(816)-$C_{104}$ to $D_5$(450)-$C_{100}$, $C_s$(574)-$C_{102}$, and $D_{3d}$(822)-$C_{104}$.** The unambiguous X-ray results reveal that the defective tubular cage $C_2$(816)-$C_{104}$ (obtained here as $La_2C_2$@$C_2$(816)-$C_{104}$) can rearrange to the other three ideal tubular cages known so far, namely, $D_5$(450)-$C_{100}$ (obtained as $La_2$@$D_5$(450)-$C_{100}$[17] and $La_2C_2$@$D_5$(450)-$C_{100}$[18]), $C_s$(574)-$C_{102}$ (obtained as $La_2C_2$@$C_s$(574)-$C_{102}$, this work), and $D_{3d}$(822)-$C_{104}$ (obtained as $Sm_2$@$D_{3d}$(822)-$C_{104}$[16]) by elimination of the pyracylene motif.

Figure 4 shows the rearrangement pathways where the partial regions of $C_2$(816)-$C_{104}$ resembling the caps of the target cages are indicated in yellow. Obviously, the two poles of $C_2$(816)-$C_{104}$ coincide exactly with those of $D_5$(450)-$C_{100}$, with the only difference between them being the pyracylene unit intercalating in the two [10]cyclacene layers. Accordingly, a direct $C_4$ loss from the pyracylene unit (hypothetical route I) converts $C_2$(816)-$C_{104}$ to $D_5$(450)-$C_{100}$. The conversion from $C_2$(816)-$C_{104}$ to $C_s$(574)-$C_{102}$ is a bit complicated by following hypothetical route II. First, $C_2$(816)-$C_{104}$ undergoes five Stone−Wales transformation steps to form an intermediate possessing one heptagon and a pair of fused-pentagons, starting with the elimination of the original pyracylene unit (see Figure S8 in the Supporting Information for details). Subsequently, extrusion of a $C_2$-unit from an indene unit sharing the pentalene pentagon forms $C_s$(574)-$C_{102}$. Consistently, the tubular $D_{3d}$(822)-$C_{104}$ cage can be formed from $C_2$(816)-$C_{104}$ via four Stone−Wales transformation steps (hypothetical route III, Figure S9 in the Supporting Information). The first step occurs on a [6, 6]-bond connecting a hexagon and a pentagon. Such a bond rotation has also been found in the formation process of a heptagon-containing $C_{96}$(NCC-3hp) cage, which is supposed to be similar to the rotation of a [6, 6]-bond in the pyrene-like fragment in nanotubes and graphene.[29,30]

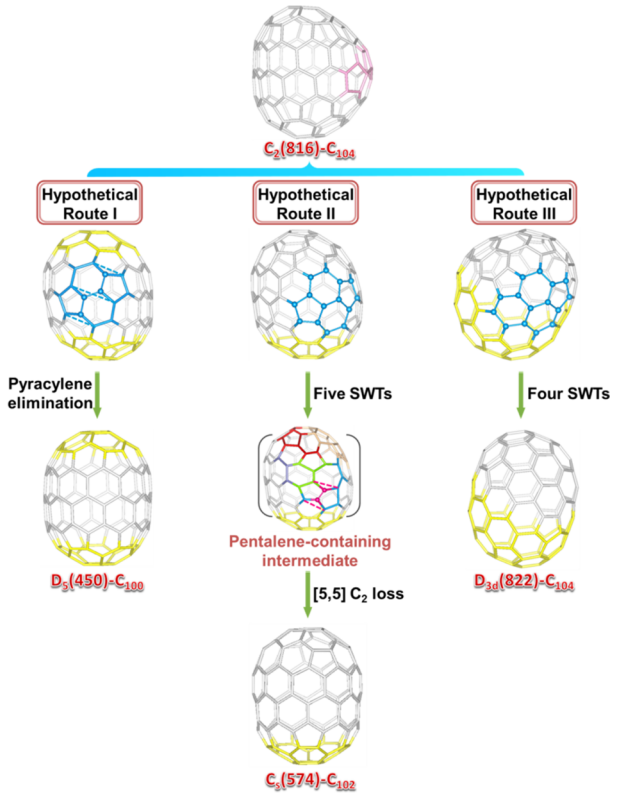


**Figure 4.** Structural rearrangement processes from the defective $C_2$(816)-$C_{104}$ cage to the other three ideal tubular fullerene cages, namely, $D_5$(450)-$C_{100}$, $C_s$(574)-$C_{102}$, and $D_{3d}$(822)-$C_{104}$. The atoms in blue indicate the starting point in the three rearrangement processes, respectively, whereas yellow emphasizes the unchanged caps. Multiple color codes are used to enhance visualization.

It is thus evident that this defective tubular cage $C_2$(816)-$C_{104}$ may be an original structure of other ideal tubular cages, presenting evidence for the "top-down" formation mechanism[31,32] of fullerenes at the atomic level, although we acknowledge that the "bottom-up" mechanism should not be ruled out. Dorn and co-workers have proposed that the asymmetric $C_1$(51383)-$C_{84}$ cage with a pair of fused-pentagons is an asymmetric intermediate which can form many well-known, high-symmetry fullerene structures via cascade shrinking processes.[33] Our results suggest that the starting point of the top-down mechanism is not merely limited to non-IPR cages, but the giant cage with a pyracylene defect, i.e., $C_2$(816)-$C_{104}$, is a "missing link" as well.

If we consider these giant fullerenes as finite-length CNTs by adding long cylindrical segments into the cage wall arbitrarily (Figure S10, Supporting Information), that is, $C_2$(816)-$C_{104}$ as an end-capped (10, 0) zigzag CNT with a pyracylene defect, $D_5$(450)-$C_{100}$ and $C_s$(574)-$C_{102}$ as short (10, 0) zigzag CNTs with different caps,[17] and $D_{3d}$(822)-$C_{104}$ as a (6, 6) armchair CNT, the transformation processes shown in Figure 4 should also be helpful to understanding the structural rearrangements from defective CNTs to ideal CNTs. Meaningfully, it is demonstrated that, even from the same starting material such as $C_2$(816)-$C_{104}$, different transformation routes would produce products with different structures (e.g., zigzag or armchair) and inherent properties (e.g., semiconducting or metallic).

## 3. CONCLUSIONS

In summary, crystallographic results of two unprecedented EMFs unambiguously established their cage structures as $La_2C_2$@$C_s$(574)-$C_{102}$ which has an ideal tubular cage and $La_2C_2$@$C_2$(816)-$C_{104}$ which has a "defective" tubular cage with a pyracylene motif in the cage waist. The relatively large cages of these two compounds provided sufficient spaces for the large $La_2C_2$ cluster to adopt a nearly planar configuration which may be an intermediate during the transformation process of $M_2C_2$ from a butterfly-like configuration to a linear structure. Moreover, our experimental results reveal for the first time that, by elimination of the pyracylene motif, the defective tubular cage $C_2$(816)-$C_{104}$ can be a starting point to form the other three known ideal tubular cages, either $D_5$(450)-$C_{100}$ and $C_s$(574)-$C_{102}$ which are short (10, 0) zigzag CNTs with


DOI: 10.1021/jacs.6b03934
J. Am. Chem. Soc. 2016, 138, 6670−6675

different caps or $D_{3d}(822)$-$C_{104}$ whose sidewall corresponds to a short (6, 6) armchair CNT, presenting evidence for the top-down formation mechanism of fullerenes.

## 4. EXPERIMENTAL SECTION

**General Instruments.** HPLC was conducted on an LC-918 machine (Japan Analytical Industry Co., Ltd.). Laser desorption/ionization time-of-flight (LDI-TOF) mass spectrometry was conducted on a BIFLEX III spectrometer (Bruker Daltonics Inc., Germany). Vis−NIR spectra were obtained with a PE Lambda 750S spectrophotometer (PerkinElmer, America) in chlorobenzene.

**Synthesis and Isolation of $La_2C_{104}$ and $La_2C_{106}$.** Soot containing lanthanum metallofullerenes was synthesized using a direct-current arc discharge method. The raw soot was refluxed in TCB under a nitrogen atmosphere for 15 h. After removal of TCB, the residue was dissolved in either toluene or chlorobenzene, and the solution was subjected to a multistage HPLC separation process. Further details are described in the Supporting Information.

**Single-Crystal X-ray Diffraction.** Crystalline blocks of $La_2C_{2n}$ ($2n$ = 104, 106) were obtained by layering a benzene solution of $Ni^{II}$(OEP) over a nearly saturated solution of the endohedral in $CS_2$ in a glass tube. Over a 20-day period, the two solutions diffused together, and black crystals formed. XRD measurements were performed at 173 K on a Bruker D8 QUEST machine equipped with a CMOS camera (Bruker AXS Inc., Germany). The multiscan method was used for absorption corrections. The structures weres solved by direct method and were refined with SHELXL-2013.[34]

*Crystal Data for $La_2C_2$@$C_s$(574)-$C_{102}$·3($CS_2$).* Data follow: $C_{107}La_2S_6$, $M_w$ = 1755.25, monoclinic, space group $P2_1/n$, $a$ = 12.3918(6) Å, $b$ = 23.9814(12) Å, $c$ = 18.4258(9) Å, $\beta$ = 95.529(1)°, $V$ = 5450.2(5) Å$^3$, $Z$ = 4, $T$ = 173(2) K, $\rho_{calcd}$ = 2.139 Mg m$^{-3}$, $\mu$(Mo K$\alpha$) = 1.851 mm$^{-1}$, 73 676 reflections measured, 15 795 unique ($R_{int}$ = 0.0292) used in all calculations. The final $wR_2$ was 0.4123 (all data) and $R_1$ (11 558 with $I > 2/s(I)$) = 0.1323. The relatively high $R_1$ and $wR_2$ values are due to the severe disorder in the cage, the metal cluster, and the intercalated solvent molecules. CCDC 1403536 contains the crystallographic data.

*Crystal Data for $La_2C_2$@$C_2$(816)-$C_{104}$·3($CS_2$).* Data follow: $C_{109}La_2S_6$, $M_w$ = 1779.27, orthorhombic, space group *Pnma*, $a$ = 24.2162(9) Å, $b$ = 18.0709(7) Å, $c$ = 12.7350(5) Å, $V$ = 5572.9(4) Å$^3$, $Z$ = 4, $T$ = 173(2) K, $\rho_{calcd}$ = 2.121 Mg m$^{-3}$, $\mu$(Mo K$\alpha$) = 1.812 mm$^{-1}$, 98 747 reflections measured, 7146 unique ($R_{int}$ = 0.0502) used in all calculations. The final $wR_2$ was 0.2801 (all data) and $R_1$ (5224 with $I > 2/s(I)$) = 0.0794. CCDC 1403537 contains the crystallographic data.

## ■ ASSOCIATED CONTENT

### Supporting Information

The Supporting Information is available free of charge on the ACS Publications website at DOI: 10.1021/jacs.6b03934.

HPLC profiles for the separation of $La_2C_2$@$C_2$(816)-$C_{104}$ and $La_2C_2$@$C_s$(574)-$C_{102}$, selected X-ray results of $La_2C_2$@$C_2$(816)-$C_{104}$ and $La_2C_2$@$C_s$(574)-$C_{102}$, structural rearrangements from $C_2$(816)-$C_{104}$ to $C_s$(574)-$C_{102}$, structural rearrangements from $C_2$(816)-$C_{104}$ to $D_{3d}$(822)-$C_{104}$, and the formation mechanisms of ideal CNTs from a defective CNT (PDF)

Additional crystal data for $La_2C_2$@$C_s$(574)-$C_{102}$·3($CS_2$) (CIF)

Additional crystal data for $La_2C_2$@$C_2$(816)-$C_{104}$·3($CS_2$) (CIF)

## ■ AUTHOR INFORMATION


### Corresponding Author

*lux@hust.edu.cn


### Notes

The authors declare no competing financial interest.

## ■ ACKNOWLEDGMENTS

Financial support from The National Thousand Talents Program of China, NSFC (Nos. 21171061 and 51472095), and Program for Changjiang Scholars and Innovative Research Team in University (IRT1014) is gratefully acknowledged. We thank the Analytical and Testing Center in Huazhong University of Science and Technology for all related measurements.

## ■ REFERENCES


(1) Lu, X.; Akasaka, T.; Nagase, S. *Angew. Chem., Int. Ed.* **2012**, *51*, 2812−2814.

(2) Yang, H.; Beavers, C. M.; Wang, Z. M.; Jiang, A.; Liu, Z. Y.; Jin, H. X.; Mercado, B. Q.; Olmstead, M. M.; Balch, A. L. *Angew. Chem., Int. Ed.* **2010**, *49*, 886−890.

(3) Wang, C. R.; Sugai, T.; Kai, T.; Tomiyama, T.; Shinohara, H. *Chem. Commun.* **2000**, 557−558.

(4) Yang, H.; Jin, H. X.; Che, Y. L.; Hong, B.; Liu, Z. Y.; Gharamaleki, J. A.; Olmstead, M. M.; Balch, A. L. *Chem. - Eur. J.* **2012**, *18*, 2792−2796.

(5) McKenzie, D. R.; Davis, C. A.; Cockayne, D. J. H.; Muller, D. A.; Vassallo, A. M. *Nature* **1992**, *355*, 622−624.

(6) Fritz, M. A.; Kemnitz, E.; Troyanov, S. I. *Chem. Commun.* **2014**, *50*, 14577−14580.

(7) Yang, S.; Wang, S.; Troyanov, S. I. *Chem. - Eur. J.* **2014**, *20*, 6875−6878.

(8) Wang, S.; Yang, S.; Kemnitz, E.; Troyanov, S. I. *Angew. Chem., Int. Ed.* **2016**, *55*, 3451−3454.

(9) Yang, S. F.; Wei, T.; Kemnitz, E.; Troyanov, S. I. *Chem. - Asian J.* **2014**, *9*, 79−82.

(10) Yang, S.; Wei, T.; Wang, S.; Ignat'eva, D. V.; Kemnitz, E.; Troyanov, S. I. *Chem. Commun.* **2013**, *49*, 7944−7946.

(11) Wang, M. Q.; Liu, J. C.; Li, W. Q.; Zhou, X.; Tian, W. Q. *J. Phys. Chem. C* **2015**, *119*, 7408−7415.

(12) Rodriguez-Fortea, A.; Alegret, N.; Balch, A. L.; Poblet, J. M. *Nat. Chem.* **2010**, *2*, 955−961.

(13) Yang, T.; Zhao, X.; Nagase, S. *Phys. Chem. Chem. Phys.* **2011**, *13*, 5034−5037.

(14) Rodriguez-Fortea, A.; Balch, A. L.; Poblet, J. M. *Chem. Soc. Rev.* **2011**, *40*, 3551−3563.

(15) Zhao, X.; Gao, W. Y.; Yang, T.; Zheng, J. J.; Li, L. S.; He, L.; Cao, R. J.; Nagase, S. *Inorg. Chem.* **2012**, *51*, 2039−2045.

(16) Mercado, B. Q.; Jiang, A.; Yang, H.; Wang, Z. M.; Jin, H. X.; Liu, Z. Y.; Olmstead, M. M.; Balch, A. L. *Angew. Chem., Int. Ed.* **2009**, *48*, 9114−9116.

(17) Beavers, C. M.; Jin, H.; Yang, H.; Wang, Z. M.; Wang, X.; Ge, H.; Liu, Z.; Mercado, B. Q.; Olmstead, M. H.; Balch, A. L. *J. Am. Chem. Soc.* **2011**, *133*, 15338−15341.

(18) Cai, W.; Bao, L.; Zhao, S.; Xie, Y.; Akasaka, T.; Lu, X. *J. Am. Chem. Soc.* **2015**, *137*, 10292−10296.

(19) Lu, X.; Akasaka, T.; Nagase, S. *Acc. Chem. Res.* **2013**, *46*, 1627−1635.

(20) Zhang, J. Y.; Fuhrer, T.; Fu, W. J.; Ge, J. C.; Bearden, D. W.; Dallas, J.; Duchamp, J.; Walker, K.; Champion, H.; Azurmendi, H.; Harich, K.; Dorn, H. C. *J. Am. Chem. Soc.* **2012**, *134*, 8487−8493.

(21) Deng, Q.; Popov, A. A. *J. Am. Chem. Soc.* **2014**, *136*, 4257−4264.

(22) Bowles, F. L.; Mercado, B. Q.; Ghiassi, K. B.; Chen, S. Y.; Olmstead, M. M.; Yang, H.; Liu, Z.; Balch, A. L. *Cryst. Growth Des.* **2013**, *13*, 4591−4598.

(23) Olmstead, M. M.; Balch, A. L.; Lee, H. M. *Acta Crystallogr., Sect. B: Struct. Sci.* **2012**, *68*, 66−70.

(24) Fowler, P. W.; Manolopoulos, D. E. *An Atlas of Fullerenes*; Dover Publications, Inc.: Mineola, NY, 1995.

(25) Campanera, J. M.; Bo, C.; Poblet, J. M. *Angew. Chem., Int. Ed.* **2005**, *44*, 7230−7233.




DOI: 10.1021/jacs.6b03934
J. Am. Chem. Soc. 2016, 138, 6670−6675

(26) Chen, C.-H.; Ghiassi, K. B.; Cerón, M. R.; Guerrero-Ayala, M. A.; Echegoyen, L.; Olmstead, M. M.; Balch, A. L. *J. Am. Chem. Soc.* **2015**, *137*, 10116−10119.
(27) Kurihara, H.; Lu, X.; Iiduka, Y.; Nikawa, H.; Hachiya, M.; Mizorogi, N.; Slanina, Z.; Tsuchiya, T.; Nagase, S.; Akasaka, T. *Inorg. Chem.* **2012**, *51*, 746−750.
(28) Nishimoto, Y.; Wang, Z.; Morokuma, K.; Irle, S. *Phys. Status Solidi B* **2012**, *249*, 324−334.
(29) Yang, S.; Wang, S.; Kemnitz, E.; Troyanov, S. I. *Angew. Chem., Int. Ed.* **2014**, *53*, 2460−2463.
(30) Dumitrică, T.; Yakobson, B. I. *Appl. Phys. Lett.* **2004**, *84*, 2775−2777.
(31) Chuvilin, A.; Kaiser, U.; Bichoutskaia, E.; Besley, N. A.; Khlobystov, A. N. *Nat. Chem.* **2010**, *2*, 450−453.
(32) Cross, R. J.; Saunders, M. *J. Am. Chem. Soc.* **2005**, *127*, 3044−3047.
(33) Zhang, J.; Bowles, F. L.; Bearden, D. W.; Ray, W. K.; Fuhrer, T.; Ye, Y.; Dixon, C.; Harich, K.; Helm, R. F.; Olmstead, M. M.; Balch, A. L.; Dorn, H. C. *Nat. Chem.* **2013**, *5*, 880−885.
(34) Sheldrick, G. M. *Acta Crystallogr., Sect. A: Found. Crystallogr.* **2008**, *A64*, 112−122.



DOI: 10.1021/jacs.6b03934
*J. Am. Chem. Soc.* 2016, 138, 6670−6675